GDCh Research Article Angewandte International Edition Chemie www.angewandte.org

How to cite: *Angew. Chem. Int. Ed.* **2025**, *64*, e202500518
doi.org/10.1002/anie.202500518

Drug Discovery

LIBX-A401: A Novel Selective Inhibitor of Acyl-CoA Synthetase Long Chain Family Member 4 (ACSL4) and Its Binding Mode

Darius Mazhari Dorooee, Séverine Ravez, Didier Vertommen, Nicolas Renault, Nicolas Papadopoulos, Romain Marteau, Emeline Charnelle, Karine Porte, Alexandre Gobert, Nathalie Hennuyer, Gaetan Herinckx, Maëla Pautric, Aurélie Jonneaux, Jean Christophe Devedjian, David Devos, Bart Staels, Patricia Melnyk, Stefan N. Constantinescu, Raphaël Frédérick, and Jamal El Bakali**

Abstract: Acyl-coenzyme A synthetase long-chain family member 4 (ACSL4), a pivotal enzyme in lipid metabolism, has emerged as a therapeutic target for ferroptosis-related conditions and cancer. However, its reference inhibitor, rosiglitazone, has off-target activity on peroxisome proliferator-activated receptor gamma (PPARγ), a key regulator of lipid homeostasis. Here, the discovery of LIBX-A401, a potent ACSL4 inhibitor derived from rosiglitazone devoid of PPARγ activity, is reported. Its binding to ACSL4 is ATP-dependent, stabilizing the C-terminal domain and altering the fatty acid gate region, as shown by Hydrogen-Deuterium Exchange Mass Spectrometry. Photoaffinity labeling identified A329 within the fatty acid binding site, while molecular dynamics and mutagenesis highlighted Q302 as critical for LIBX-A401 binding. LIBX-A401 exhibits anti-ferroptotic properties in cells, supported by target engagement. These findings establish LIBX-A401 as a valuable tool to study ACSL4 in ferroptosis and cancer, while its elucidated binding mode paves the way for the rational design of improved inhibitors.

Introduction

Lipid metabolism encompasses a series of dynamic and interdependent processes that regulate the synthesis, storage, and use of lipids in living organisms. Within this complex set of biochemical processes, the acyl-coenzyme A (acyl-CoA) synthetase long-chain family of enzymes (ACSLs) plays a pivotal role in the activation of long-chain fatty acids into corresponding fatty acyl-CoA esters. Once activated, fatty acids participate in various cellular pathways, including the synthesis of phospholipids (PLs), triacylglycerol and cholesterol esters, β-oxidation, and protein acylation.[1] In mammals, the ACSL family comprises five members, ACSL1 and ACSL3-6, which have different tissue and subcellular distributions and substrate preferences.[2–4] They have all been identified as potential therapeutic targets in various diseases.[5,6] More specifically, ACSL4 recently emerged as an attractive target in some cancers, including hepatocellular carcinoma,[7]

[*] D. Mazhari Dorooee, R. Marteau, K. Porte, R. Frédérick
Medicinal Chemistry Research Group (CMFA), Louvain Drug Research Institute (LDRI), Université Catholique de Louvain, 73 Avenue Mounier, B1.73.10, Brussels 1200, Belgium
E-mail: raphael.frederick@uclouvain.be

S. Ravez, E. Charnelle, A. Gobert, M. Pautric, A. Jonneaux, J. C. Devedjian, D. Devos, P. Melnyk, J. El Bakali
Univ. Lille, Inserm, CHU Lille, UMR-S-U1172 – LilNCog – Lille Neuroscience & Cognition, Lille F-59000, France
E-mail: jamal.el-bakali@univ-lille.fr

D. Vertommen, G. Herinckx
MASSPROT Platform, de Duve Institute, Université Catholique de Louvain, Brussels, Belgium

N. Renault
INSERM, CHU Lille, U-1286 – INFINITE – Institute for Translational Research in Inflammation, Université de Lille, Lille F-59000, France

N. Papadopoulos, S. N. Constantinescu
Ludwig Institute for Cancer Research, Brussels, Belgium

N. Papadopoulos, S. N. Constantinescu
de Duve Institute, Université catholique de Louvain, Brussels, Belgium

N. Papadopoulos, S. N. Constantinescu
WELBIO Department, WEL Research Institute, Wavre, Belgium

N. Hennuyer, B. Staels
Univ. Lille, Inserm, CHU Lille, Institut Pasteur de Lille, U-1011-EGID, Lille F-59000, France

M. Pautric, A. Jonneaux, J. C. Devedjian, D. Devos
Department of Medical Pharmacology, Expert Center of Parkinson's Disease, ALS and neurogenetic, LICEND COEN Center Lille, Lille F-59000, France

S. N. Constantinescu
Ludwig Institute for Cancer Research, Nuffield Department of Medicine, Oxford University, Oxford, UK

Additional supporting information can be found online in the Supporting Information section

estrogen receptor-negative breast cancer,[8–10] and prostate cancer.[11,12] Indeed, recent studies highlight the critical role of ACSL4 in tumor progression and metastasis. For instance, in androgen receptor-independent prostate cancer, ACSL4 overexpression sustains dysregulated fatty acid (FA) metabolism, promoting cell proliferation and invasion.[11] In triple-negative breast cancer, ACSL4 upregulation drives phospholipid remodeling, enhancing membrane fluidity and activating integrin $\beta 1$, contributing to metastasis.[8] Similarly, in ovarian cancer, ACSL4 facilitates metastasis by increasing polyunsaturated fatty acid (PUFA)-lipid content, which enhances invasiveness.[13] These findings underscore the potential of ACSL4 as a therapeutic target, particularly in metastatic cancers. In addition, due to its marked preference for PUFAs, ACSL4 has been identified as a pivotal contributor to ferroptosis,[14–19] an iron-dependent regulated cell death characterized by extensive membrane lipid peroxidation.[20,21] Ferroptosis is implicated in various pathologies, and its inhibition holds therapeutic potential for conditions such as ischemia-reperfusion injuries[22] as well as neurodegenerative diseases like Alzheimer's disease and Parkinson's disease.[23] ACSL4 drives ferroptosis by enriching membrane PLs with PUFAs, which are highly susceptible to peroxidation.[16,17] Interestingly, genetic depletion or pharmacological inhibition of ACSL4 confers a strong protection against ferroptosis.[16] Therefore, inhibiting ACSL4 may have a positive impact on diseases or conditions in which ferroptosis is involved, as well as in certain cancers.

So far, while a few molecules have been described, no potent, selective, and well-characterized ACSL4 inhibitor has been identified.[24–27] The most widely used ACSL4 inhibitor is rosiglitazone (ROSI), which selectively inhibits ACSL4 (over other ACSLs) in the micromolar range.[28] However, its potent activity on peroxisome proliferator-activated receptor gamma (PPARγ), a nuclear receptor strongly involved in lipid metabolism and the mediation of ROSI's antidiabetic effects, constitutes an important limitation due to off-target effects and associated safety concerns. These drawbacks underscore the need for developing novel ACSL4 inhibitors that specifically avoid these limitations. However, a major challenge in this effort is the lack of structural information about ACSL4 and its related family members, which would aid rational inhibitor design. Indeed, although mammalian ACSLs have been thoroughly biochemically characterized, structural information is missing, with the only known structure of ACSL being the one of *Thermus thermophilus* *tt*LC-FACS.[29] Despite sharing only ≈20% sequence identity (37% sequence similarity) with human ACSL4, this structure provides the first glimpse into the ACSL architecture and mechanism of catalysis. Indeed, this bacterial ACSL acts as a dimeric complex of two identical subunits displaying a large *N*-terminal domain linked via a six amino acid linker to a relatively short and flexible *C*-terminal domain, with the active site located at the domain interface. An important feature in the structure of ACSLs is the presence of an FA gate domain, whose sequence (D-x4-Y/W-LPLAH-x2-E) is highly conserved in mammals.[2] Interestingly, *tt*LC-FACS was shown to function through a Bi Uni Uni Bi ping-pong mechanism, where ATP binds first, inducing the opening of the FA tunnel, allowing FA binding and subsequent acyl-AMP formation and PPi release.[29] In the second step, CoA reacts with acyl-AMP to generate acyl-CoA and AMP as products. These mechanistic and structural data are crucial for understanding the functioning of human ACSLs. However, the specific intricacies of ACSL's architecture and their ligand-binding sites remain largely unknown.

Hydrogen-Deuterium Exchange Mass Spectrometry (HDx-MS) and photoaffinity labeling (PAL) are powerful techniques contributing to the elucidation of the structural basis of important proteins. HDx-MS provides a dynamic view of the conformational changes in proteins upon inhibitor binding and could help identify potential binding regions.[30–32] On the other hand, PAL enables the covalent attachment of a probe to the protein target, allowing for precise mapping of the ligand-binding site.[33,34]

Here, we report i) the medicinal chemistry approach around ROSI leading to sub-micromolar range inhibitors of human ACSL4 devoid of PPARγ activity, ii) the chemical biology approach, combining HDx-MS and PAL to gain structural insights into the binding mode of these inhibitors and iii) the cellular evaluation of the most promising compound demonstrating ACSL4-dependent anti-ferroptotic properties.

Results and Discussion

In order to draw an early structure-activity relationship (SAR), ROSI analogs were purchased or readily synthesized as described in Scheme S1. Inhibitory activity was evaluated on the human recombinant ACSL4 using the Enzchek pyrophosphate assay as previously described.[35] Thus, we started our SAR study by evaluating commercial thiazolidinedione analogs and by modulating the western side chain of ROSI (Table S1 and Scheme S1). Building upon these initial modulations, we selected both ROSI (Compound **1**, IC_{50} = 1.1 μM) and its phenyl analog (Compound **2**, IC_{50} = 0.4 μM) as the starting points for further SAR investigations (Table 1 and Schemes S2 and S3). Our goal was to enhance the inhibitory activity against ACSL4 while minimizing the effect on PPARγ. Our initial step involved removing the thiazolidinedione ring, a key moiety responsible for the PPARγ activity of ROSI. However, this modification resulted in a complete loss of inhibitory activity against ACSL4 (**3**, IC_{50} > 50 μM). Next, *N*-methylation of thiazolidinedione was performed to remove the acidic character essential for PPARγ activity. Encouragingly, the *N*-methyl analog (**4**), known to be inactive against PPARγ,[36] retained micromolar-range activity against ACSL4 (IC_{50} = 4.5 μM), hence demonstrating the possibility of abolishing PPARγ activity while maintaining the ACSL4 inhibitory potency. We then envisaged ester compounds as ring-opened analogs of the thiazolidinedione moiety. The ester **5**, which displays an ethylene linker, retained micromolar-range activity. In contrast, increasing or decreasing the length of the linker resulted in a reduction (**6**) or loss (**7**) of inhibitory activity (Table 1). Notably, rigidifying the ethylene linker of compound **5** leads to cinnamic derivative **8** with a potency comparable to

Table 1: SAR investigation around the thiazolidinedione moiety of ROSI. IC_{50} values (± SD) were determined by three independent experiments performed in duplicate for each compound concentration.

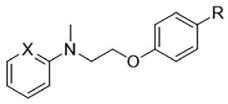

Entry	X	R	ACSL4 IC_{50}, μM
1 (ROSI)	N	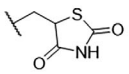	1.1 ± 0.1
2	CH		0.4 ± 0.1
3	N	H	> 50
4	N	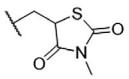	4.5 ± 1.1
5	CH	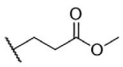	8.5 ± 3.5
6	CH	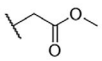	24.1 ± 0.6
7	CH	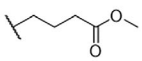	> 50
8	CH	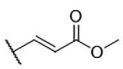	1.5 ± 0.6

rosiglitazone (IC_{50} = 1.5 μM) with high selectivity over ACSL3 (IC_{50} > 50 μM), which shares 63% sequence identity with ACSL4. Remarkably, compound **8** was inactive on PPARγ at 10 μM, in contrast to rosiglitazone, which displays an EC_{50} of 36 nM. Finally, replacing the amine in the linker connecting the two phenyl groups with an amide, resulting in compound **9**, allowed for a further improvement of ACSL4 inhibitory activity (IC_{50} = 0.38 μM, Figure 1a) while keeping the same selectivity profile as compound **8**. Compound **9** features a Michael acceptor that may potentially engage in an irreversible mechanism. However, the reversibility of the inhibition was demonstrated using a rapid dilution assay (Figure S1A). Furthermore, **9** demonstrates minimal reactivity with thiols such as glutathione (GSH) from pH 6.5 to 8.5 and beta-mercaptoethanol (BME) at pH 7.4, as analyzed by HPLC-MS (Figure S1C–F). We also confirmed compound stability by HPLC-MS from pH 6.5 to 8.5 and in cell culture medium (DMEM, Figure S1B).

The binding of compound **9** to ACSL4 was further confirmed using two biophysical techniques, namely nano Differential Scanning Fluorimetry (nDSF) and MicroScale Thermophoresis (MST). As illustrated in Figure 1, no binding event was detected when **9** was tested in the absence of ATP against ACSL4 using these two techniques (Figure 1b,c). However, in the presence of a saturating concentration of

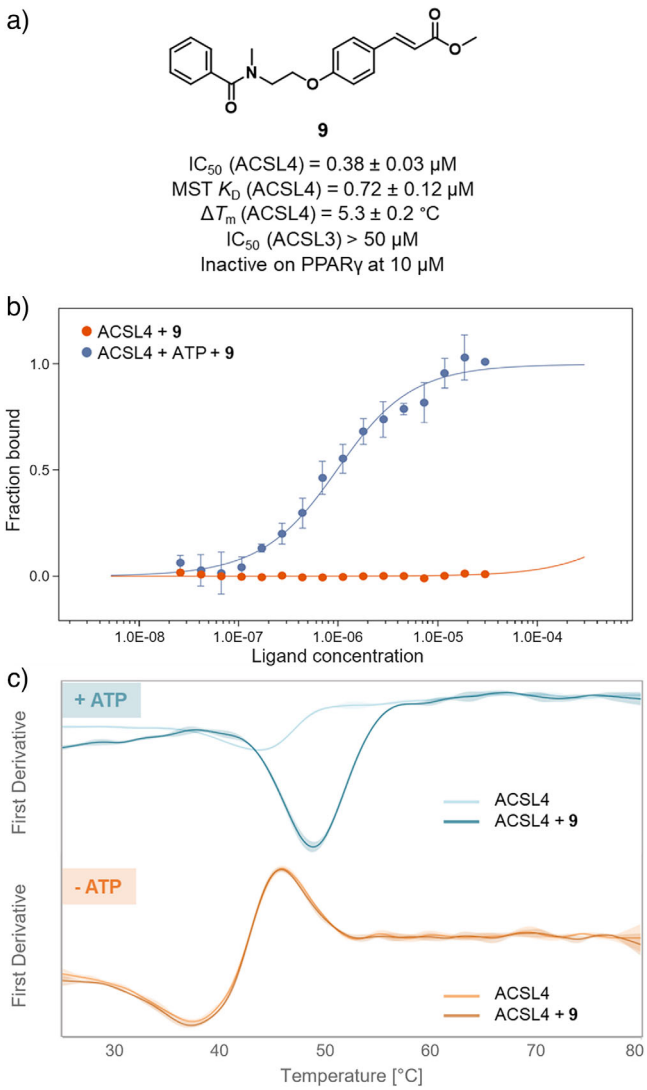

Figure 1. Evaluation of compound **9** against ACSL4. a) Structure of **9** and summary of its binding and inhibitory activity profile against ACSL4 as well as its selectivity over ACSL3 and PPARγ. b) MST traces, with and without 1 mM ATP (in blue and orange, respectively), showing that the binding of **9** to ACSL4 depends on the prior binding of ATP. A K_D value of 720 nM was obtained for **9** in the presence of 1 mM ATP. c) nDSF traces with and without 1 mM ATP (in blue and orange, respectively), confirming that ATP is required for the binding of compound **9**. A ΔT_m value of 5.3 °C was obtained for **9** (5 μM) in the presence of 1 mM ATP. K_D and ΔT_m values (± SD) were determined by three independent experiments for each compound concentration. Curves in panels B and C are shown as the mean ± SD values. IC_{50} values (± SD) were determined by three independent experiments performed in duplicate for each compound concentration.

ATP, a ΔT_m value of 5.3 °C was obtained by nDSF (at 5 μM of **9**), and a K_D value of 0.72 μM was determined by MST. These data indicate that binding of **9** is ATP-dependent, consistent with observations from *tt*LC-FACS, where ATP binding induces the opening of the fatty acid tunnel, facilitating FA binding. Taken together, these findings suggest that compound **9** interacts with ACSL4 in a manner analogs to FAs, following a similar ATP-dependent binding mechanism.

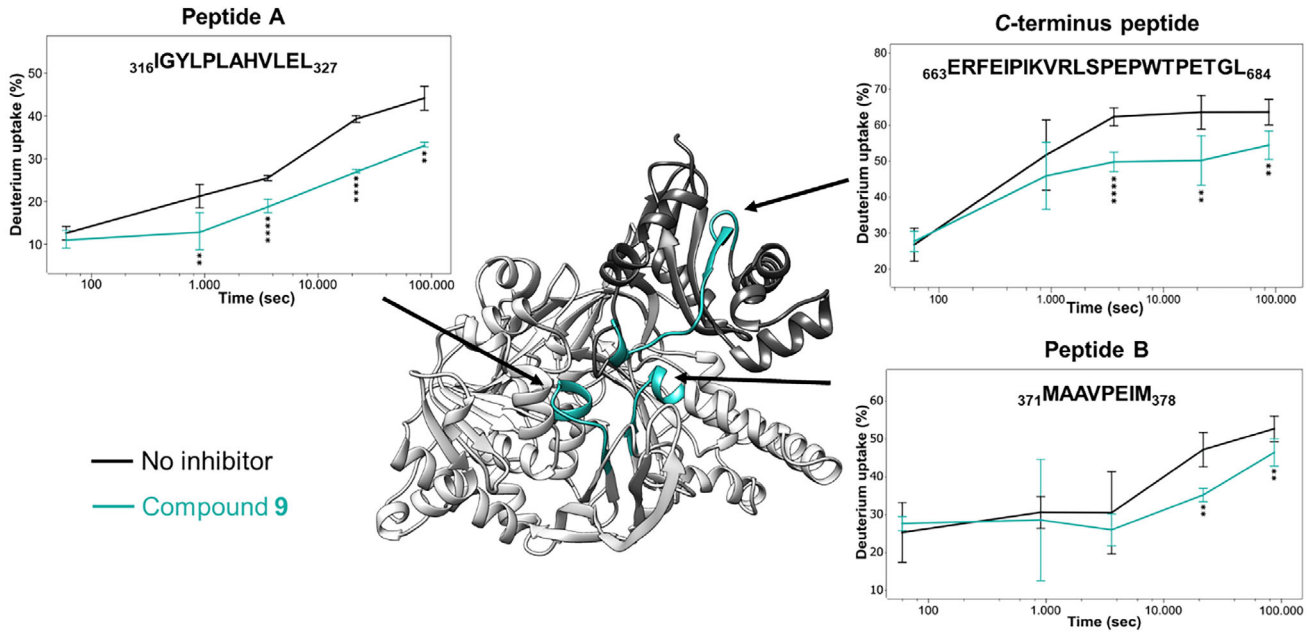

Figure 2. HDx-MS results with compound **9** in the presence of ATP. Changes in deuterium uptake at different exchange times are presented for the identified peptides, which are mapped onto the refined AlphaFold model of ACSL4. *C*-terminus and *N*-terminus of ACSL4 are depicted in dark gray and white, respectively. Peptides A and B, along with a selected peptide in the *C*-terminal region closest in proximity to these two, are shown in cyan. Uptake plots for each illustrated peptide show the impact of compound **9** on deuterium incorporation. Peptide traces shown represent mean ± SD of three independent experiments. Statistically significant using *t*-test from HDExaminer, $^{**}p < 0.01$, $^{***}p < 0.001$, $^{****}p < 0.0001$.

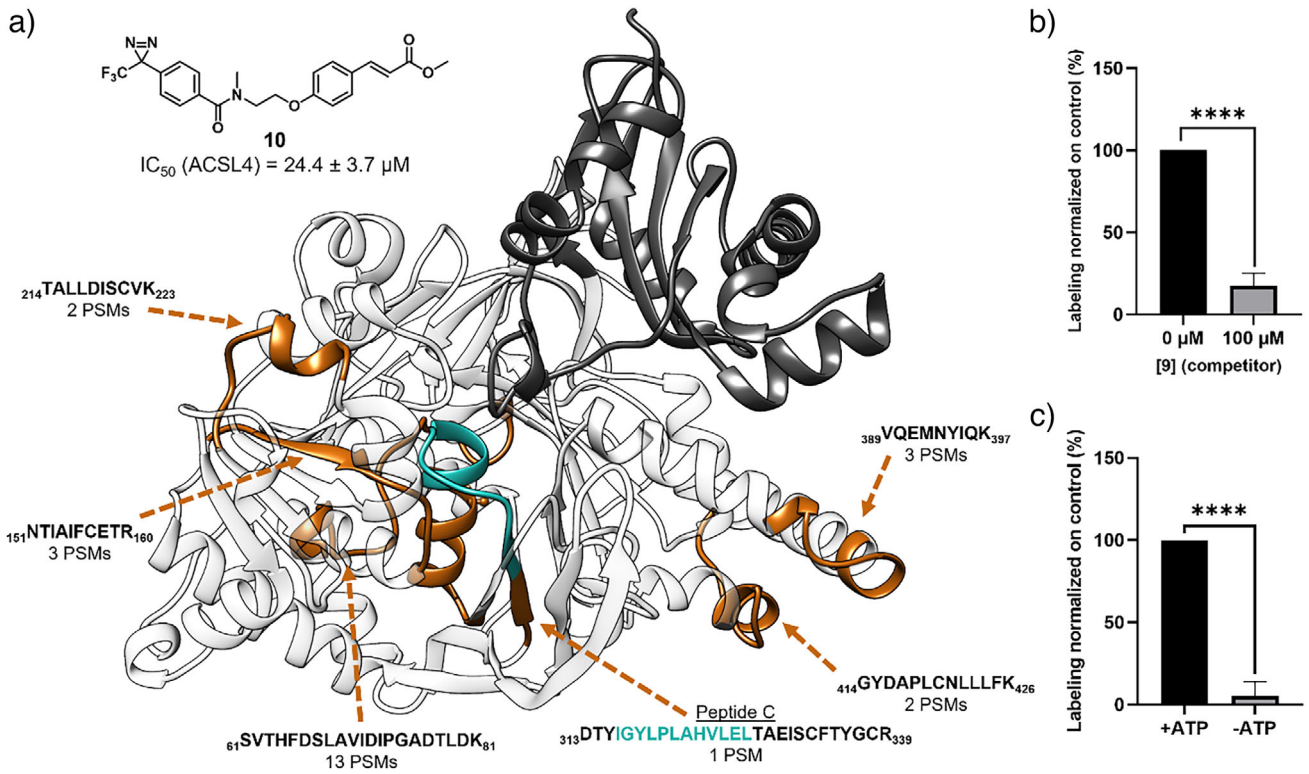

Figure 3. Photoaffinity labeling identification of compound **9** binding site in ACSL4. a) The structure of photoaffinity labeling probe **10** and representation of its binding peptides (orange) on the refined AlphaFold ACSL4 model for which the number of peptide-spectrum matches (PSMs) identified are shown. The previously identified peptide A, included in identified peptide C, is represented in cyan. b) Results of the competition assay in targeted MS/MS analysis for peptide C with and without compound **9**. c) Results of the labeling assay with and without ATP in targeted MS/MS analysis for peptide C. Data shown are representative of three independent experiments. Graphs in panels B and C are shown as the mean ± SD values. Statistically significant using unpaired *t*-test, $^{****}p < 0.0001$.

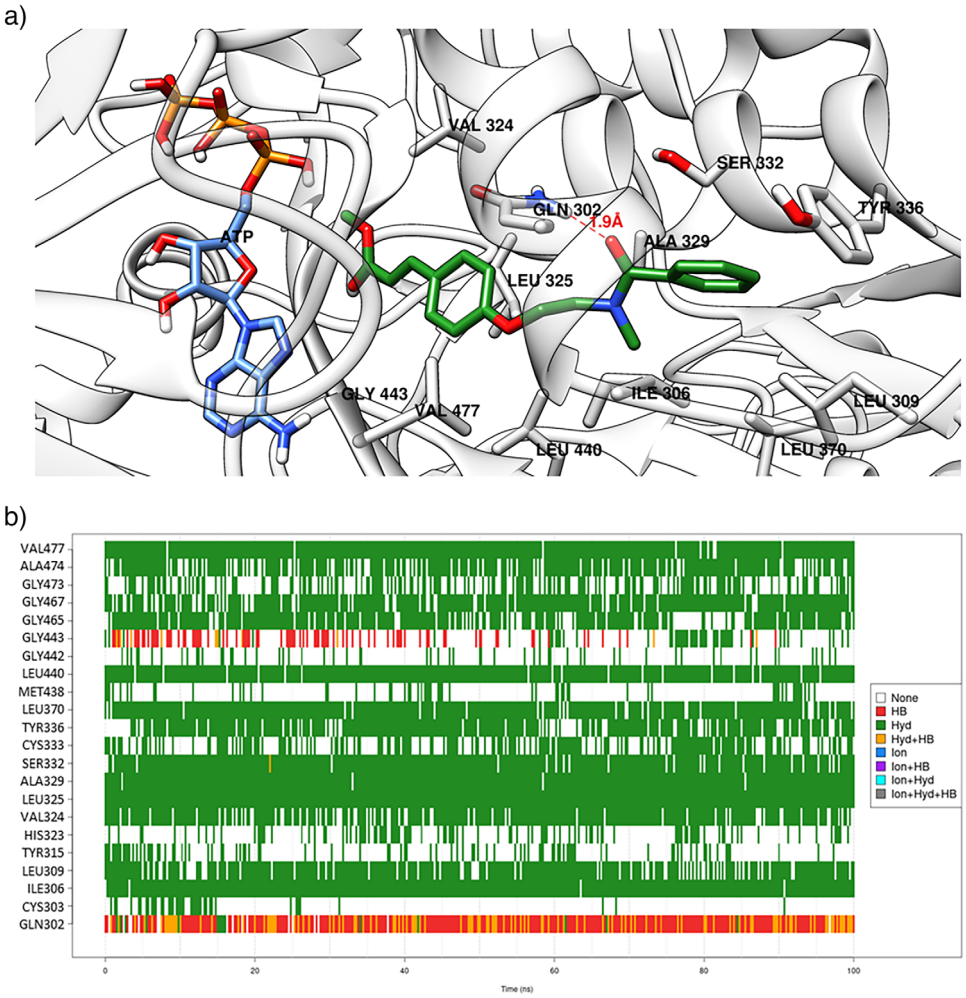

Figure 4. Putative binding mode of compound **9** on ACSL4. a) ASCL4-compound **9** complex after docking and an additional 100 ns MD simulation. b) Representative trace of the contacts that compound **9** forms with the ACSL4 model during the 100 ns MD simulation, showing that compound **9** primarily interacts through hydrophobic contacts and hydrogen bonds with Q302. Each vertical line corresponds to an intermolecular contact, and the color is associated with the interaction type (e.g., green corresponds to a hydrophobic contact and red to a hydrogen bond).

In the absence of structural data, we set out to elucidate the binding mode of compound **9**. To this end, two powerful and complementary techniques were used: HDx-MS and PAL. Because of the measurement of deuterium incorporation on the peptide amide backbone by MS, HDx-MS allows for the identification of protein domains that are exposed to solvent and, therefore is well suited to unveil protein conformational changes upon ligand binding as well as identifying potential binding sites.[36] The on-column pepsin digestion led to at least 82% of protein coverage with assayed conditions (Figure S2). nDSF confirmed ACSL4 stability at exchange temperature for the longest exchange time (24 h, Figure S3). Because ATP is required for the binding of **9**, we first compared the differences in peptide deuterium intake between ACSL4 with and without a saturating concentration of ATP (400 μM, ACSL4-ATP). The addition of ATP resulted in reduced accessibility of the *C*-terminus domain to deuterium incorporation (Figure S4A), consistent with the literature, where ATP binding to *tt*LC-FACS was shown to induce locking of the *C*-terminus domain onto the *N*-terminus domain.[29] Next, we aimed to investigate the impact of compound **9** binding on the conformation of ACSL4. Consequently, we compared two conditions: one where ACSL4 was incubated with ATP at 400 μM (ACSL4-ATP), and another where ACSL4 was present with both ATP at 400 μM and compound **9** at 25 μM (saturating concentration, ACSL4-ATP-**9**). Figure 2 and Figure S4B indicate that ACSL4-ATP-**9** further reduces the deuterium uptake in the *C*-terminus domain compared to ACSL4-ATP. In addition, the presence of compound **9** resulted in a significant reduction in deuterium uptake on two other sequences: peptide $_{316}$IGYLPLAHVLEL$_{327}$ (peptide A) and peptide $_{371}$MAAVPEIM$_{378}$ (peptide B). Interestingly, peptide A sequence contains the highly conserved FA gate domain (Figure S5) previously described as important for substrate specificity.[2–4] The refined model of ACSL4 (described below) presented in Figure 2 shows that the two identified peptides are positioned close to each other and near the *C*-terminus domain, suggesting the possibility of a potential binding site for molecule **9** within this region.

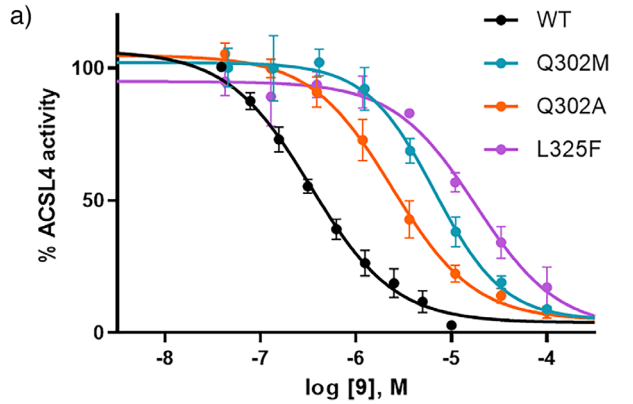

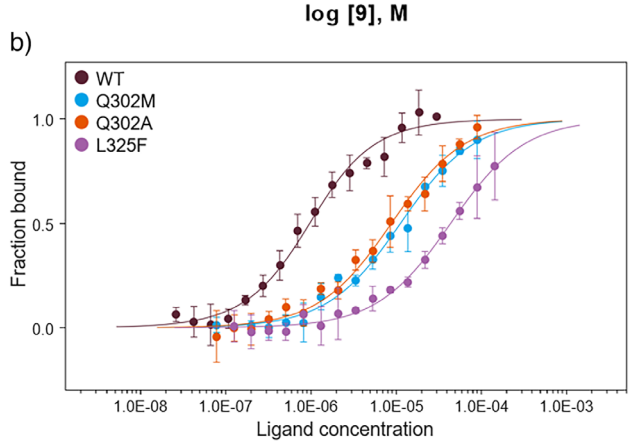

c)

ACSL4	Compound **9**	
	IC_{50} (μM)	K_D (μM)
WT	0.38 ± 0.03	0.72 ± 0.12
Q302M	7.1 ± 0.6	11.0 ± 1.6
Q302A	2.4 ± 0.4	8.6 ± 1.3
L325F	17.8 ± 3.8	43.5 ± 5.4

Figure 5. Impact of site-directed mutations on the inhibitory activity and affinity of compound **9** for ACSL4. a) Inhibition profiles of compound **9** against wild-type ACSL4 and selected mutants (Q302A in orange, Q302 M in blue, and L325F in purple) showing that the site-directed mutations affect inhibitory activity of **9**. b) Binding curves from MST experiments showing the impact of site-directed mutations (Q302A in orange, Q302 M in blue, and L325F in purple) on the affinity of compound **9** for ACSL4. c) Table summarizing IC_{50} and K_D values (± SD) of compound **9** against wild-type ACSL4 and selected mutants. IC_{50} values and curves were determined by three independent experiments performed in duplicate for each compound concentration. Similarly, K_D values and curves were determined by three independent experiments for each compound concentration. Curves in panels B and C are shown as the mean ± SD values.

To further define the binding site of compound **9**, we conducted PAL experiments. Based on the SAR (data not shown), we designed an original photoactivable probe, introducing a trifluoromethyl diazirine group at the *para* position of the benzamide part on **9** to give the probe **10** (Figure 3a). The latter was synthesized from amine **11** following a standard BOP coupling procedure in the presence of the commercial 4-[3-(trifluoromethyl)-3*H*-diazirin-3-yl]benzoic acid (Scheme S4). Although less potent than **9**, probe **10** retained some inhibitory activity against ACSL4 (IC_{50} = 24.4 μM). Next, ACSL4 was incubated with probe **10** at 100 μM for 30 min, and the photoaffinity labeling was then performed by irradiation at 365 nm for 10 min. To determine the crosslinking site, the samples underwent trypsin digestion, and the resulting peptides were analyzed using nanoUPLC-MS/MS (sequence coverage = 73%, Figure S6). Following this experimental setup, five peptides were detected with an increase in peptide mass of 419.13 Da corresponding to the incorporation of the probe (Figure 3a; Figure S7C and Table S2). Interestingly, the peptide with the amino acid sequence $_{313}$DTYIGYLPLAHVLELTAEISCFTYGCR$_{339}$ (Peptide C) comprises the sequence of peptide A identified by HDx-MS. Based on these results, we performed targeted MS/MS analysis in the presence or absence of 100 μM of competing compound **9** to highlight non-specific labeling. The signal of peptide C was significantly decreased upon the addition of **9** (Figure 3b; Figure S7D), while other identified peptides showed either smaller or no significant decreases (Figure S7A).

To validate these results, we measured the labeling of identified peptides with and without ATP as we demonstrated the requirement of ATP for the binding of **9**. The inability to identify peptide C as labeled in the absence of ATP further confirmed the labeling specificity of this peptide (Figure 3c; Figure S7B,D). Finally, analysis of the MS/MS fragmentation profile designated A329 as the modified residue of the identified peptide (Figure S8). It is worth noting that A329 in human ACSL4 aligns with L236 of *tt*LC-FACS (Figure S5), which is located at the distal end of the FA tunnel. Interestingly, mutation of this specific amino acid in the rat ACSL4 to either glutamate or glutamine led to a dramatic loss in enzymatic activity.[37]

Building upon these findings, we initiated in silico studies to elucidate the binding mode of compound **9**. A BLAST search of PDB templates revealed 16 homologous sequences with at least 50% coverage and 25% sequence identity with human ACSL4. Therefore, we employed AlphaFold 2.0[38] to restrain the extensive set of structural templates to predict the structure of the soluble form of human ACSL4 (42–711). The design of a model for the ACSL4-ligand complex was facilitated by utilizing the unbound state of the AlphaFold model and the conserved ATP position found in homologous PDB structures. Arachidonic acid was selected as the preferential ligand to identify the orthosteric binding pocket through docking and energy refinement, utilizing the arachidonyl-AMP intermediate formed during the enzymatic reaction. Once the arachidonyl-AMP was removed, blind docking experiments were conducted to explore the entire protein. These experiments revealed the best docking pose of **9** within the orthosteric FA binding site, yielding a docking score of -9.76 kcal mol^{-1}. Other docking poses were observed (Figure S9) but with docking scores lowered by at least 10%. Interestingly, the best docking pose is consistent with the PAL experiments showing the labeling of A329, a residue predicted to be part of the FA tunnel. To refine the model of the ASCL4-**9** complex, molecular dynamics (MD) simulations were carried out during triplicated 100 computed nanoseconds (Figure 4; Figure S10). All criteria satisfied a convergence in terms of energy relaxation and stabilization of the gyration radius of the ACSL4-ATP-**9** complex. During this

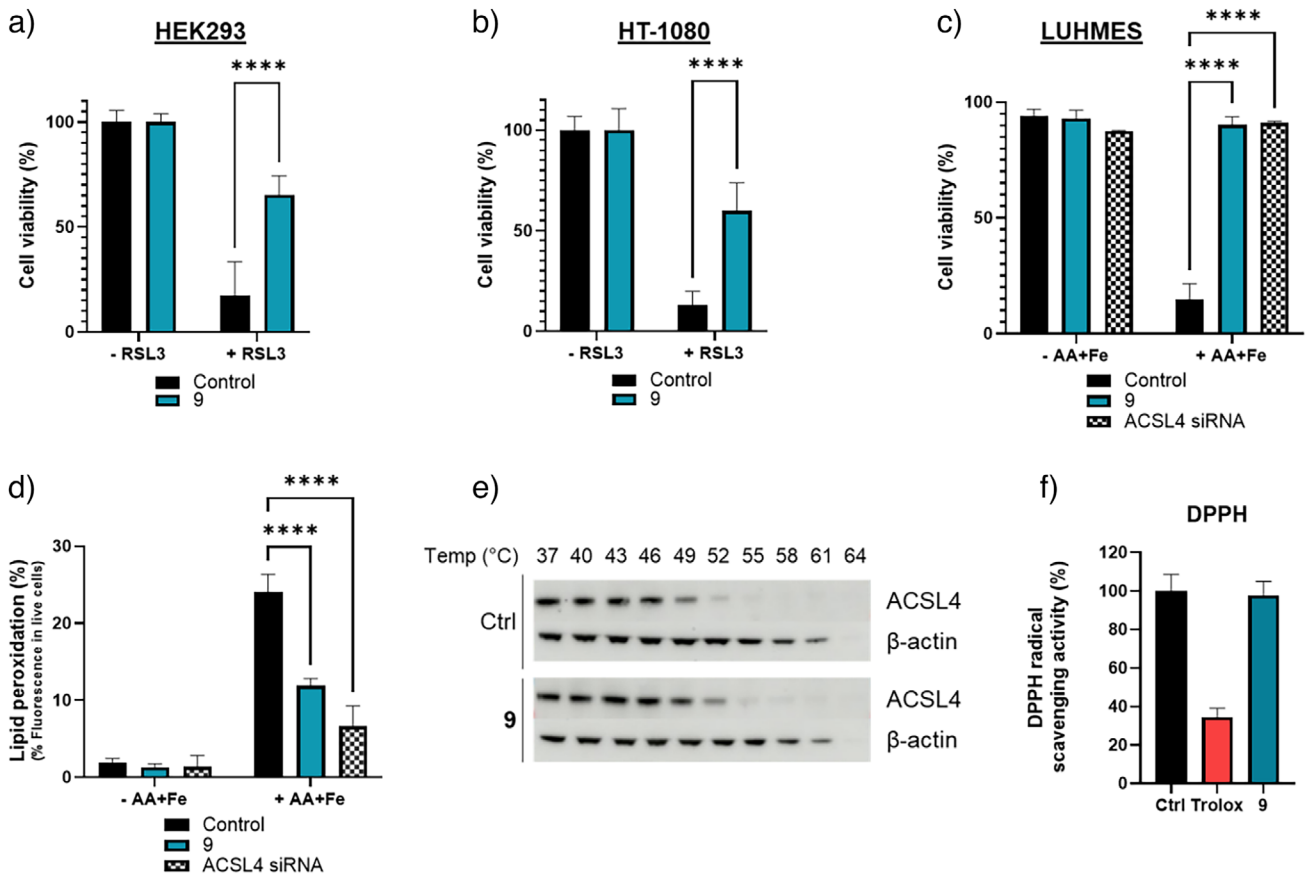

Figure 6. Compound **9** protects cells from ferroptosis. a) Cell viability analysis of HEK293 cells pretreated with 2.5 μM of **9** for 24 h, followed by treatment with RSL3 for 48 h. Data represent mean and SD ($n = 4$). Statistical analysis was performed using Tukey's multiple comparisons test. ****$p < 0.001$. b) Cell viability analysis of HT-1080 cells pretreated with 2.5 μM of **9** for 24 h, followed by treatment with RSL3 for 48 h. Data represent mean and SD ($n = 4$). Statistical analysis was performed using Tukey's multiple comparisons test. ****$p < 0.001$. c) Cell viability analysis of LUHMES cells transfected with ACSL4 siRNA or pretreated with 2.5 μM of **9** for 4 h, followed by treatment with AA + Fe for 48 h. Data represent mean and SD ($n = 3$). Statistical analysis was performed using Tukey's multiple comparisons test. ****$p < 0.001$. d) Percentage of lipid peroxidation in LUHMES cells transfected with ACSL4 siRNA or pretreated with 2.5 μM of **9** for 4 h, followed by treatment with AA + Fe for 24 h. Lipid peroxidation in cells was measured by flow cytometry using the C11 BODIPY 581/591 probe. The staining data obtained at 530 nm (oxidized C11 BODIPY 581/591) are plotted as a histogram. Data represents mean and SEM ($n = 4$). Statistical analysis was performed using Tukey's multiple comparisons test. ****$p < 0.001$. e) Representative western blots showing the thermal stability of ACSL4 in LUHMES cells treated with either DMSO or 10 μM compound **9**. ACSL4 levels were quantified by immunoblotting. From three independent experiments, T_m values of 48.3 ± 0.5 °C (DMSO) and 50.9 ± 0.1 °C (compound **9**) were determined, corresponding to a ΔT_m of 2.6 ± 0.6 °C. f) Evaluation of radical-trapping antioxidant activity of **9** (50 μM) compared to trolox (50 μM) using the DPPH assay. Data represent mean and SD ($n = 3$).

100 ns MD-based energy relaxation, compound **9** interacts by sustained hydrogen bonds with Q302 side chain and, to a lesser extent, with the backbone of G443. Other interatomic attractions are hydrophobic contacts with the lipophilic tunnel exhibiting residues L325, V324, A329, L440, V477, and L468 (Figure 4; Figure S10).

Interestingly, among ACSLs, only ACSL4 exhibits a glutamine at position 302 (Figure S5). In contrast, ACSL3, for which compound **9** does not display any inhibitory activity, displays a methionine at this position. Thus, to verify the significance of Q302 in the potency and affinity of compound **9** for ACSL4, ACSL4(Q302A) and ACSL4(Q302 M) mutants were generated, followed by an evaluation of their enzymatic activities and kinetic parameters (Figure S11). Only the ACSL4(Q302 M) protein exhibited activity comparable to wild-type ACSL4, whereas ACSL4(Q302A) maintained ≈80% of the enzymatic activity.

To our satisfaction, the introduction of the ACSL4(Q302 M) mutation increased the IC_{50} value of **9** by 18 fold (IC_{50} ACSL4(Q302M) = 7.1 μM) and the K_D value by 15 fold, confirming the importance of Q302 in the binding of **9** (Figure 4). A similar trend was observed with ACSL4(Q302A). Additionally, we mutated L325 since this residue is predicted to be located in the middle of the FA tunnel. This residue is part of both identified peptides A and C and was shown to be important for the binding of **9** through hydrophobic interactions with the central phenyl ring (Figure 5). Interestingly, ACSL1, 5, and 6 display a phenylalanine residue at this position. Thus, we investigated the ACSL4(L325F) mutant, assuming that the bulky phenylalanine would sterically affect the binding of **9** into the FA tunnel. The ACSL4(L325F) mutant maintained ≈60% activity (Figure S11), and the introduction of this mutation led to ≈50 fold increase of IC_{50} and K_D values for

9. These results further corroborate the binding of **9** into the FA tunnel.

Next, we assessed the cytotoxicity of compound **9** across six different cell lines (SiHa, HCT-116, MDA-MB-231, HEK293, HT-1080, and LUHMES). Compound **9** demonstrated minimal toxicity at concentrations up to 10 μM (Figure S12). Given that ACSL4 is a key enzyme in triggering ferroptosis, its inhibition represents a promising strategy to block this iron-dependent form of cell death, which is implicated in important diseases such as Parkinson's disease.[23] Hence, the anti-ferroptotic potential of compound **9** was evaluated in HEK293, HT-1080, and LUHMES cell lines, which are commonly used to study ACSL4 in the context of ferroptosis.[39–41] RSL3 was used to induce ferroptosis in HEK293 and HT-1080 cells. LUHMES cells, a non-oncogenic model of human dopaminergic neurons widely used in Parkinson's disease research and highly sensitive to ferroptosis, were treated with a combination of arachidonic acid (AA) and iron (Fe), which better mimics the neuropathological environment.[41] Compound **9** at 2.5 μM significantly prevented RSL3-induced cell death in both HEK293 (Figure 6a) and HT-1080 cells (Figure 6b). Additionally, in LUHMES cells, compound **9** (2.5 μM) effectively inhibited cell death caused by AA + Fe treatment, comparable to the protective effect seen with ACSL4 knockdown (Figure 6c; Figure S13). Given the relevance of LUHMES cells as a model for neurodegenerative diseases, further experiments were conducted in this system. The protective effect of compound **9** was correlated to a significant decrease in lipid peroxidation to a similar level to ACSL4 siRNA (Figure 6d). Additionally, target engagement was confirmed by evaluating the thermal stability of ACSL4 in the presence of compound **9**, which enhanced ACSL4's thermal stability by increasing its resistance to unfolding by 2.6 °C (Figure 6e).

Finally, we excluded any potential contribution of radical-trapping antioxidant activity to the observed anti-ferroptotic effect by performing a classical DPPH assay (Figure 6f).

Collectively, these findings strongly support that compound **9** prevents ferroptotic cell death by engaging and inhibiting ACSL4.

Conclusion

In summary, starting from ROSI, we designed novel submicromolar ACSL4 inhibitors that are selective against ACSL3 and devoid of PPARγ activity. We demonstrated that the binding of **9**, our best compound in this series, is dependent on the prior binding of ATP to ACSL4. HDx-MS experiments indicated that ATP binding induces a significant stabilization of the *C*-terminus domain. This effect was even more pronounced in the presence of **9,** which further impacted the conformation of two other peptide sequences, one of which (peptide A) delineates the FA gate domain. PAL experiments based on diazirine-based probe **10** identified residue A329, an amino acid predicted to be part of the FA pocket. Complementary MD simulations pointed to residue Q302 as a key amino acid for the binding of **9** through H-bonding. Site-directed mutagenesis supported this hypothesis, as mutation of Q302 induced a significant decrease in the potency and affinity of **9** to ACSL4. Cellular evaluations demonstrated that compound **9** protects HEK293, HT-1080, and LUHMES cells from ferroptosis. Target engagement for compound **9** further supports the role of ACSL4 in its anti-ferroptotic activity. Overall, compound **9** (LIBX-A401) is a promising tool for studying ACSL4 in ferroptosis-related diseases and cancer, and the elucidation of its binding mode paves the way to the rational design of optimized inhibitors.

Author Contributions

D.M.D. performed conceptualization, methodology, formal analysis, investigation, data curation, visualization, and wrote the original draft. S.R. performed conceptualization, validation, formal analysis, investigation, data curation, visualization, supervision, project administration, funded acquisition, and wrote, reviewed, and edited the final manuscript. D.V. performed methodology, validation, formal analysis, investigation, data curation, and supervision. N.R. performed methodology, validation, formal analysis, investigation, data curation, visualization, and wrote the original draft. N.P. performed methodology, formal analysis, investigation, and data curation. R.M. performed formal analysis, investigation, and data curation. E.C., K.P., A.G., and N.H. performed formal analysis, investigation, and data curation. G.H. performed Investigation and data curation. M.P. performed investigation, data curation, and visualization. A.J. and J.C.D. performed investigation and data curation. D.D., B.S., P.M., and S.N.C. funded acquisition and wrote, reviewed, and edited the final manuscript. R.F. performed conceptualization, validation, supervision, project administration, funded acquisition, and wrote, reviewed, and edited the final manuscript. J.E.B. performed conceptualization, validation, formal analysis, investigation, data curation, visualization, supervision, project administration, funded acquisition, and wrote, reviewed, and edited the final manuscript.

Acknowledgements

The authors thank Prof. Jean-François Goossens for providing access to the Varioskan Flash spectrophotometer. The 500 and 300 MHz NMR facilities were funded by the Région Haut-de-France, the Fonds Européens de Développement Régional (FEDER), the Ministère de l'Enseignement supérieur, de la Recherche et de l'Innovation (MESRI), and Université de Lille. The HDx-MS platform was supported by a grant from the Fondation contre le Cancer (Ref: 3758) awarded to S.N.C. This work was supported by l'Agence Nationale de la Recherche (ANR-23-CE18-0051) (EGID, ANR-10-LABX-046), the French Community Of Belgium (ARC 21/26–115), the Belgian Fonds National de la Recherche Scientifique (F.R.S.-FNRS; PDR grant 40003810), the Télévie (Grant 40007387) and the Région Hauts-de-France (Start-AIRR FerInh4Park). E.C. is a recipient of a Ph.D fellowship from the University of Lille and the Région Hauts-de-France.

D.M.D. is a Télévie research fellow. N.P. received an Aspirant Ph.D Fellowship from FRS-FNRS (Belgium).

Conflict of Interests

The authors declare no conflict of interest.

Data Availability Statement

The data that support the findings of this study are available in the supplementary material of this article. This also includes further references. [42–48]

Keywords: ACSL4 inhibitors • Ferroptosis • Hydrogen Deuterium Exchange (HDx) mass spectrometry • Parkinson's disease • Photoaffinity labeling

[1] T. J. Grevengoed, E. L. Klett, R. A. Coleman, *Annu. Rev. Nutr.* **2014**, *34*, 1–30.
[2] P. A. Watkins, D. Maiguel, Z. Jia, J. Pevsner, *J. Lipid. Res.* **2007**, *48*, 2736–2750.
[3] E. Soupene, F. A. Kuypers, *Exp. Biol. Med. (Maywood).* **2008**, *233*, 507–521.
[4] E. L. Klett, S. Chen, A. Yechoor, F. B. Lih, R. A. Coleman, *J. Lipid. Res.* **2017**, *58*, 884–894.
[5] J. Quan, A. M. Bode, X. Luo, *Eur. J. Pharmacol.* **2021**, *909*, 174397.
[6] Z. Wu, J. Sun, Z. Liao, J. Qiao, C. Chen, C. Ling, H. Wang, *Front. Neurosci.* **2022**, *16*, 1030512.
[7] J. Grube, M. M. Woitok, A. Mohs, S. Erschfeld, C. Lynen, C. Trautwein, T. Otto, *Cell Death Dis.* **2022**, *13*, 704.
[8] Y. Qiu, X. Wang, Y. Sun, T. Jin, R. Tang, X. Zhou, M. Xu, Y. Gan, R. Wang, H. Luo, M. Liu, X. Tang, *Cancer Res.* **2024**, *84*, 1856–1871.
[9] M. E. Monaco, *Oncotarget* **2023**, *14*, 563–575.
[10] J. Lin, P. Zhang, W. Liu, G. Liu, J. Zhang, M. Yan, Y. Duan, N. Yang, *Elife* **2023**, *12*, RP87510.
[11] Y. Ma, X. Zhang, O. A. Alsaidan, X. Yang, E. Sulejmani, J. Zha, Z. Beharry, H. Huang, M. Bartlett, Z. Lewis, H. Cai, *Mol. Cancer Res.* **2021**, *19*, 124–135.
[12] P. H. A. Cao, A. Dominic, F. E. Lujan, S. Senthilkumar, P. K. Bhattacharya, D. E. Frigo, E. Subramani, *Nat. Rev. Urol.* **2024**, *21*, 615–637.
[13] Y. Wang, M. Hu, J. Cao, F. Wang, J. R. Han, T. W. Wu, L. Li, J. Yu, Y. Fan, G. Xie, H. Lian, Y. Cao, N. Naowarojna, X. Wang, Y. Zou, *Cell* **2025**, *188*, 412–429.e27.
[14] S. J. Dixon, G. E. Winter, L. S. Musavi, E. D. Lee, B. Snijder, M. Rebsamen, G. Superti-Furga, B. R. Stockwell, *ACS Chem. Biol.* **2015**, *10*, 1604–1609.
[15] H. Yuan, X. Li, X. Zhang, R. Kang, D. Tang, *Biochem. Biophys. Res. Commun.* **2016**, *478*, 1338–1343.
[16] S. Doll, B. Proneth, Y. Y. Tyurina, E. Panzilius, S. Kobayashi, I. Ingold, M. Irmler, J. Beckers, M. Aichler, A. Walch, H. Prokisch, D. Trümbach, G. Mao, F. Qu, H. Bayir, J. Füllekrug, C. H. Scheel, W. Wurst, J. A. Schick, V. E. Kagan, J. P. Angeli, M. Conrad, *Nat. Chem. Biol.* **2017**, *13*, 91–98.
[17] V. E. Kagan, G. Mao, F. Qu, J. P. F. Angeli, S. Doll, C. S. Croix, H. H. Dar, B. Liu, V. A. Tyurin, V. B. Ritov, A. A. Kapralov, A. A. Amoscato, J. Jiang, T. Anthonymuthu, D. Mohammadyani, Q. Yang, B. Proneth, J. Klein-Seetharaman, S. Watkins, I. Bahar, J. Greenberger, R. K. Mallampalli, B. R. Stockwell, Y. Y. Tyurina, M. Conrad, H. Bayır, *Nat. Chem. Biol.* **2017**, *13*, 81–90.
[18] H. L. Zhang, B. X. Hu, Z. L. Li, T. Du, J. L. Shan, Z. P. Ye, X. D. Peng, X. Li, Y. Huang, X. Y. Zhu, Y. H. Chen, G. K. Feng, D. Yang, R. Deng, X. F. Zhu, *Nat. Cell. Biol.* **2022**, *24*, 88–98.
[19] Z. Li, Z. M. Xu, W. P. Chen, X. J. Du, C. X. Ou, Z. K. Luo, R. Wang, C. Q. Zhang, C. D. Ge, M. Han, F. Wang, R. R. He, W. Y. Sun, J. Ma, X. Y. Liang, Z. W. Liu, *Nat. Chem. Biol.* **2024**, *20*, 1341–1352.
[20] S. J. Dixon, K. M. Lemberg, M. R. Lamprecht, R. Skouta, E. M. Zaitsev, C. E. Gleason, D. N. Patel, A. J. Bauer, A. M. Cantley, W. S. Yang, B. Morrison 3rd, B. R. Stockwell, *Cell* **2012**, *149*, 1060–1072.
[21] B. R. Stockwell, *Cell* **2022**, *185*, 2401–2421.
[22] Y. Chen, H. Fan, S. Wang, G. Tang, C. Zhai, L. Shen, *Front. Cell Dev. Biol.* **2021**, *9*, 688605.
[23] S. K. Ryan, C. L. Ugalde, A. S. Rolland, J. Skidmore, D. Devos, T. R. Hammond, *Trends Pharmacol. Sci.* **2023**, *44*, 674–688.
[24] Q. Huang, Y. Ru, Y. Luo, X. Luo, D. Liu, Y. Ma, X. Zhou, M. Linghu, W. Xu, F. Gao, Y. Huang, *Sci. Adv.* **2024**, *10*, eadk1200.
[25] W. Yan, D. Wang, N. Wan, S. Wang, C. Shao, H. Zhang, Z. Zhao, W. Lu, Y. Tian, H. Ye, H. Hao, *Anal. Chem.* **2022**, *94*, 14820–14826.
[26] A. F. Castillo, U. D. Orlando, P. M. Maloberti, J. G. Prada, M. A. Dattilo, A. R. Solano, M. M. Bigi, M. A. Ríos Medrano, M. T. Torres, S. Indo, G. Caroca, H. R. Contreras, B. E. Marelli, F. J. Salinas, N. R. Salvetti, H. H. Ortega, P. Lorenzano Menna, S. Szajnman, D. E. Gomez, J. B. Rodríguez, E. J. Podesta, *Cell. Mol. Life Sci.* **2021**, *78*, 2893–2910.
[27] J. Duan, Z. Wang, R. Duan, C. Yang, R. Zhao, Q. Feng, Y. Qin, J. Jiang, S. Gu, K. Lv, L. Zhang, B. He, L. Birnbaumer, S. Yang, Z. Chen, Y. Yang, *Hepatology* **2022**, *75*, 140–153.
[28] J. H. Kim, T. M. Lewin, R. A. Coleman, *J. Biol. Chem.* **2001**, *276*, 24667–24673.
[29] Y. Hisanaga, H. Ago, N. Nakagawa, K. Hamada, K. Ida, M. Yamamoto, T. Hori, Y. Arii, M. Sugahara, S. Kuramitsu, S. Yokoyama, M. Miyano, *J. Biol. Chem.* **2004**, *279*, 31717–31726.
[30] D. D. Weis, *Hydrogen Exchange Mass Spectrometry of Proteins*. John Wiley & Sons, Hoboken, New Jersey **2016**.
[31] L. Konermann, J. Pan, Y. H. Liu, *Chem. Soc. Rev.* **2011**, *40*, 1224–1234.
[32] G. R. Masson, J. E. Burke, N. G. Ahn, G. S. Anand, C. Borchers, S. Brier, G. M. Bou-Assaf, J. R. Engen, S. W. Englander, J. Faber, R. Garlish, P. R. Griffin, M. L. Gross, M. Guttman, Y. Hamuro, A. J. R. Heck, D. Houde, R. E. Iacob, T. J. D. Jørgensen, I. A. Kaltashov, J. P. Klinman, L. Konermann, P. Man, L. Mayne, B. D. Pascal, D. Reichmann, M. Skehel, J. Snijder, T. S. Strutzenberg, E. S. Underbakke, et al., *Nat. Methods* **2019**, *16*, 595–602.
[33] E. Smith, I. Collins, *Future Med. Chem.* **2015**, *7*, 159–183.
[34] O. Laselva, Z. Qureshi, Z. W. Zeng, E. V. Petrotchenko, M. Ramjeesingh, C. M. Hamilton, L. J. Huan, C. H. Borchers, R. Pomès, R. Young, C. E. Bear, *iScience* **2021**, *24*, 102542.
[35] R. Marteau, S. Ravez, D. Mazhari Dorooee, H. Bouchaoui, K. Porte, J. C. Devedjian, P. Melnyk, D. Devos, R. Frédérick, J. El Bakali, *Biochem. Pharmacol.* **2022**, *204*, 115239.
[36] K. Liu, R. M. Black, J. J. Acton 3rd, R. Mosley, S. Debenham, R. Abola, M. Yang, R. Tschirret-Guth, L. Colwell, C. Liu, M. Wu, C. F. Wang, K. L. MacNaul, M. E. McCann, D. E. Moller, J. P. Berger, P. T. Meinke, A. B. Jones, H. B. Wood, *Bioorg. Med. Chem. Lett.* **2005**, *15*, 2437–2440.
[37] L. Stinnett, T. M. Lewin, R. A. Coleman, *Biochim. Biophys. Acta* **2007**, *1771*, 119–125.
[38] J. Jumper, R. Evans, A. Pritzel, T. Green, M. Figurnov, O. Ronneberger, K. Tunyasuvunakool, R. Bates, A. Z˘ídek, A. Potapenko, A. Bridgland, C. Meyer, S. A. A. Kohl, A. J. Ballard, A. Cowie, B. Romera-Paredes, S. Nikolov, R. Jain, J. Adler,

T. Back, S. Petersen, D. Reiman, E. Clancy, M. Zielinski, M. Steinegger, M. Pacholska, T. Berghammer, S. Bodenstein, D. Silver, O. Vinyals, et al., *Nature* **2021**, *596*, 583–589.
[39] L. Magtanong, G. D. Mueller, K. J. Williams, M. Billmann, K. Chan, D. A. Armenta, L. E. Pope, J. Moffat, C. Boone, C. L. Myers, J. A. Olzmann, S. J. Bensinger, S. J. Dixon, *Cell Chem. Biol.* **2022**, *29*, 1409–1418.e6.
[40] L. Mahoney-Sanchez, H. Bouchaoui, I. Boussaad, A. Jonneaux, K. Timmerman, O. Berdeaux, S. Ayton, R. Krüger, J. A. Duce, D. Devos, J. C. Devedjian, *Cell Rep.* **2022**, *40*, 111231.
[41] H. Bouchaoui, L. Mahoney-Sanchez, G. Garçon, O. Berdeaux, L. Y. Alleman, D. Devos, J. A. Duce, J. C. Devedjian, *Free Radical Biol. Med.* **2023**, *195*, 145–157.
[42] B. Staels, W. Koenig, A. Habib, R. Merval, M. Lebret, I. Pineda Torra, P. Delerive, A. Fadel, G. Chinetti, J. C. Fruchart, J. Najib, J. Maclouf, *A. Nature* **1998**, *393*, 790–793.
[43] C. V. Goemans, D. Vertommen, R. Agrebi, J. F. Collet, *Mol. Cell* **2018**, *70*, 614–627.e7.
[44] A. T. McNutt, P. Francoeur, R. Aggarwal, T. Masuda, R. Meli, M. Ragoza, J. Sunseri, D. R. Koes, *J. Cheminform.* **2021**, *13*, 43.
[45] E. Krieger, G. Vriend, *Bioinformatics* **2014**, *30*, 2981–2982.
[46] B. Do Van, F. Gouel, A. Jonneaux, K. Timmerman, P. Gelé, M. Pétrault, M. Bastide, C. Laloux, C. Moreau, R. Bordet, D. Devos, J. C. Devedjian, *Neurobiol. Dis.* **2016**, *94*, 169–178.
[47] S. L. Gaonkar, H. Shimizu, *Tetrahedron* **2010**, *66*, 3314–3317.
[48] R. G. Giles, N. J. Lewis, J. K. Quick, M. J. Sasse, M. W. J. Urquhart, L. Youssef, *Tetrahedron* **2000**, *56*, 4531–4537.

Manuscript received: January 07, 2025
Revised manuscript received: February 21, 2025
Accepted manuscript online: February 27, 2025
Version of record online: March 18, 2025